Received: September 10, 2022. Revised: December 12, 2022.

INASS

International Journal of
Intelligent Engineering & Systems

http://www.inass.org/

Novel Virtual Speed Sensor Design for Fault-Tolerant Vector Control for Induction Motor Drives Based on the Non-Linear Unscented Kalman Filter

Marouane Rayyam[1]* **Malika Zazi[1]**

[1]*Department of Electrical Engineering, Mohammed V University in Rabat, ENSAM, Rabat, Morocco*
* Corresponding author's Email: rayyam.marouane@gmail.com

Abstract: The design of electrical drives capable of tolerating sensor faults has recently become very popular due to their possible use in Fault Tolerant Control systems. This paper introduces a virtual speed sensor design based on a nonlinear state estimation algorithm for fault-tolerant vector control for Induction Motor Drives after speed sensor faults. The rotor speed estimator is realized by integrating the Unscented Kalman Filter (UKF) and the Sliding Mode Observer (SMO) based only on the measurements of the stator current and voltage. This proposal is dedicated to maintain the proper behaviour of the Indirect Rotor Field Oriented Control of the induction motor drive, where it is necessary to switch to the nonlinear estimators as a result of damage to the speed encoder. Simulation studies of the proposed fault tolerant design are performed in the case of total and partial losses of the speed sensor in a closed loop control structure for different operating conditions of the drive system. Fault-tolerant designs based on the UKF and the SMO estimators show good performance in the presence of speed sensor faults in terms of stability, overshoot rate (less than 10%), and trajectory tracking over low and medium speed range. However, the SMO performance is reduced for high-speed operation (ωr >1400rpm) over the UKF which maintain good performance over the entire speed range.

Keywords: Diagnosis, Estimation, Fault tolerant control, Sliding mode observer, Unscented Kalman filter.

Notation list

$\boldsymbol{i_s^d / i_s^q}$: Stator current in d / q axes
$\boldsymbol{\varphi_r^d / \varphi_r^q}$: Rotor flux in d / q axes
$\boldsymbol{\omega_r}$ / $\boldsymbol{\omega_{rf}}$: Real / Faulty rotor speed measurement
$\boldsymbol{R_s}$ / $\boldsymbol{R_r}$: Stator / Rotor resistance
$\boldsymbol{L_s}$ / $\boldsymbol{L_r}$ / $\boldsymbol{M}$: Stator / Rotor/ Mutual inductance
$\boldsymbol{\tau_r}$ / $\boldsymbol{\tau_s}$: Rotor/Stator time constant
$\boldsymbol{J}$: Rotor inertia
$\boldsymbol{p}$: Pole-pair number
$\boldsymbol{T_e}$: Sampling time
$\boldsymbol{X_k / Y_k / U_k}$: State/output/input vector at step k
$\boldsymbol{\sigma_{k^+}^i}$: ith sigma point at step k
$\boldsymbol{\sigma_{f,k^-}^i}$: Projected sigma point using the function f
$\boldsymbol{\hat{X}_{k^+}}$ / $\boldsymbol{\hat{X}_{k^-}}$: State estimate/prediction at step k
$\boldsymbol{K_k}$: Kalman gain at step k
$\boldsymbol{P_{k^+}}$: The covariance matrix at step k
$\mathbf{P_{zz,k}}$: Covariance matrix of innovations
$\mathbf{P_{xz,k}}$: The cross-covariance matrix between the state estimate errors and innovations
$\boldsymbol{W^i}$: Weight associated with the *ith* sigma point
$\boldsymbol{Q / R}$: Covariance matrix of state/measurement noise

1. Introduction

Today's demand for reliability and safety has been increased in most automation control. Consequently, it is necessary to develop control systems that have the ability to self-adjust to malfunctions and maintain overall system stability and availability while maintaining acceptable and satisfactory performance [1, 2].

In most industrial systems, the use of sensors is unavoidable [1, 3]. They provide the controllers with the required data to make decision. However, these sensors are subject to numerous failures, which affect system performance [3, 4]. In vector-controlled Induction Motor Drive (IMD) systems,

current and voltage sensors are required to ensure the proper operation of the control strategy. Usually, these components are sensitive and can break. The performance of the IMD with estimation algorithms remains stable even if they do not utilize the physical voltage sensor, but they cannot work properly without the data from the stator current sensors [5]. Rotor speed sensor is considered as the main important sensor used in the IMD. The accuracy of the signal from this component is crucial, but very sensitive to the current drive and weather conditions [3] which leads to unsatisfactory behavior of the whole system. Consequently, the topology of the system must be changed if the speed sensor is damaged [6, 7].

The classical methods for detecting sensor faults were based on hardware redundancy [8, 9], so that the signals from the faulty sensors are compared to the generated fault indicators to detect fault occurrence. Once the fault is confirmed, a reconfiguration action is made to eliminate the fault. Hardware redundancy is simple and direct, but very expensive and a heavy solution. The use of additional components increases the complexity of the whole system and poses numerous diagnostic problems [7, 10].

With the discovery of electronic computers, model-based approaches have attracted researcher's consideration. This has led to adopting the concept of analytical redundancy where virtual sensors (estimators, filters, and observers) have been employed to estimate rotor speed, internal states, and machine parameters [11, 12] using the inputs and outputs of the system [13, 15].

In order to maintain acceptable performance and preserve the stability of the whole IMD with faulty speed sensor, a variety of Fault Tolerant Control (FTC) strategies have been proposed. These strategies are mainly divided into two groups: Passive-FTC (PFTC) and Active-FTC (AFTC) [16]. In PFTC approaches, faults are handled as limited non-structural uncertainties [17, 18]. The design of the control scheme is required to be robust only to specified faults. Thus, fault detection and estimation issues are also not involved. Contrary to PFTC, AFTC would require an FDI block in order to estimate, detect and isolate fault signals [19].

To detect speed sensor faults, most diagnostic methods use the difference between the measured and the estimated rotor speed signals. When this error exceeds the selected threshold, the detection algorithm confirms the occurrence of faults in the speed sensor. Recently, a number of published papers have appeared in the literature documenting the FTC of the speed sensor, as in [20]. In this paper, authors have applied the EKF to compare rotor speed measurements and their estimates to diagnose the state of the speed sensor. Furthermore, the authors have proposed hybrid-EKF and GIMC design for the reconfiguration actions. In [21], authors have applied the adaptive stator flux observer to estimate the rotor speed. Based on the error between the measured and estimated speed signals, the FDI algorithm makes decision regarding the occurrence or non-occurrence of a malfunctioning condition. At the same time, the error is refined by a low-pass filter and checked against the selected threshold. Authors in [22] integrate the MLV algorithm for detecting and isolating speed sensor faults. In this algorithm, the likelihood coefficients of a feedback measured speed using the physical sensor and two virtual signals from the EKF and ELO are integrated to diagnose the occurrence of a speed fault and maintain the normal operation of the drive system for a wide speed range. Authors in [18], have utilized the stator currents to evaluate the health of the mechanical speed encoder. This technique permitted to separate the reconfiguration and diagnosis steps so that the estimated currents are used for fault detection step, and the speed sensorless control is used in the reconfiguration step.

The main contribution of this work is to perform an effective virtual speed sensor design for fault-tolerant vector controlled IMD with faulty speed sensor based on the use of the Unscented Kalman Filter (UKF) algorithm. This algorithm is considered as the minimum mean square error and the reduced computational burden. Synthesized UKF algorithm was used to estimate, detect and isolate the speed sensor fault in order to maintain the stability and the normal behaviour of the IRFOC IMD system even if the speed sensor is damaged. To improve the validity of the proposed diagnosis algorithm, the UKF algorithm was compared with the SMO algorithm (detailed in the appendix) in term of stability and trajectory tracking.

The rest of this work is organized as follows: SECTION 2 introduces the IM dynamic model and details the SMO and the UKF algorithms for IM state estimation, SECTION 3 presents the FTC design for speed sensor fault-tolerant vector control of IMD, and SECTION 4 provides simulation results of the proposed FTC structure.

2. State estimation of the Induction Motor (IM)

2.1 Nonlinear state estimation observers

IM state space representation Eq. (1) is established by considering the equations of state for stator currents, rotor flux and rotation speed in the d/q reference frame rotating with the synchronous speed ω_s. The model is controlled by the stator voltage and load torque. The chosen output variables are the stator currents as in Eq. (2) [10].

$$\begin{cases} \dot{X} = AX + BU + V \\ Y = CX + DX + W \end{cases} \tag{1}$$

With

$$X = \begin{bmatrix} i_s^d \\ i_s^q \\ \varphi_r^d \\ \varphi_r^q \\ \omega_r \end{bmatrix} \quad U = \begin{bmatrix} u_s^d \\ u_s^q \\ C_r \end{bmatrix} \quad Y = \begin{bmatrix} i_s^d \\ i_s^q \end{bmatrix} \tag{2}$$

Where u_s^{dq} and i_s^{dq} represents the stator voltage and the current in d/q axis; φ_r^{dq} is the d/q axis rotor flux; ω_r is the rotor speed; C_r is the load torque; $A \in \mathbb{R}^{n\times n}$ refers to the state matrix; $B \in \mathbb{R}^{n\times m}$ is the input matrix; $C \in \mathbb{R}^{p\times n}$ is the output matrix; $X \in \mathbb{R}^n$ is the state vector; $U \in \mathbb{R}^m$ is the control input vector; $Y \in \mathbb{R}^p$ is the output vector; $V \in \mathbb{R}^n$ and $W_k \in \mathbb{R}^n$ are the process and measurement noises ; $(n, m, p) \in \mathbb{N}$ are the number of states, number of inputs and the number of outputs, respectively.

The continuous form in Eq. (1) is discretized by the first-order Euler approximation Eq. (3). The detailed discrete state space form of the IM is as in Eq. (4).

$$A_k = e^{AT_e} \approx I + AT_e,\ B_{k=}\, BT_e \tag{3}$$

$$X_{k+1} = \underbrace{\begin{bmatrix} 1+\alpha T_e & \omega_s T_e & \frac{\beta T_e}{\tau_r} & \beta\omega_r T_e & 0 \\ -\omega_s T_e & 1+\alpha T_e & -\beta\omega_r T_e & \frac{\beta T_e}{\tau_r} & 0 \\ \frac{MT_e}{\tau_r} & 0 & 1-\frac{T_e}{\tau_r} & \omega_{rl} T_e & 0 \\ 0 & \frac{MT_e}{\tau_r} & -\omega_{rl} T_e & 1-\frac{T_e}{\tau_r} & 0 \\ 0 & 0 & -\gamma T_e i_{sq} & \gamma T_e i_{sd} & 1-\frac{fT_e}{J} \end{bmatrix}_k}_{A_k} X_k + \underbrace{\begin{bmatrix} \delta & 0 & 0 \\ 0 & \delta & 0 \\ 0 & 0 & 0 \\ 0 & 0 & 0 \\ 0 & 0 & -\frac{p}{J} T_e \end{bmatrix}}_{B_k} U_k + V_k$$

$$Y_k = \underbrace{\begin{bmatrix} 1 & 0 & 0 & 0 & 0 \\ 0 & 1 & 0 & 0 & 0 \end{bmatrix}}_{C_k} \times X_k + W_k \tag{4}$$

The following factorizations have been adopted to simplify the state equations:

$$\alpha = -\frac{1}{\sigma}\left(\frac{1}{\tau_s} + \frac{1-\sigma}{\tau_r}\right), \beta = \frac{1-\sigma}{\sigma M},$$
$$\delta = \frac{T_e}{\sigma L_s}, \sigma = 1 - \frac{M^2}{L_s L_r}, \gamma = \frac{p^2 M}{J L_r} \tag{5}$$

Where $R_s(R_r)$ is the stator (rotor) resistance; $L_s(L_r)$ and M are the stator (rotor) and the mutual inductances; p is the number of pole pairs; J is the total inertia; f is the friction coefficient; τ_r is the rotor time constant; σ is the total leakage coefficient; T_e is the sampling time.

2.2 Unscented Kalman filter (UKF)

The Unscented Kalman Filter (UKF) is a non-linear estimation algorithm proposed by Julier and Uhlmann [9]. It differs from the Extended Kalman Filter by the fact that its algorithm does not require the step of linearization of the non-linear *f*-transition and *h*-measurement functions. It therefore allows to surmount the tedious and delicate calculation problem of Jacobian matrices in certain cases [10]. Its principle relies on the Unscented Transformation (UT), which allows the successive calculation of the mean and the posteriori covariance of the state, by

creating a finite number of points called "Sigma points", which depend on the size of the state vector.

The operating steps of the UKF algorithm are as follows:

- Compute the 2n+1 sigma points to be propagated, noted σ_k^i and composed of 2n+1 state vector. These sigma points are obtained by:

$$\sigma_{k-1^+}^{i} = \begin{cases} \hat{X}_{k-1^+} , & i = 0 \\ \hat{X}_{k-1^+} + \sqrt{(n+\gamma)P_{k-1^+}}|_i & 1 \le i \le n \\ \hat{X}_{k-1^+} - \sqrt{(n+\gamma)P_{k-1^+}}|_{i+n} & n+1 \le i \le 2n \end{cases} \quad (6)$$

Where $\sigma_{k^+}^{i} \in \mathbb{R}^{n \times 2n+1}$ are the sigma points at time k; n is the dimension of the state vector; γ is a scaling parameter; x_i corresponds to the ith column of the matrix x.

- Transform sigma points using system dynamics

$$\sigma_{f,k^-}^{i} = f_k(\sigma_{k-1^+}^{i}, U_k) \quad (7)$$

- Set the weight vector

$$W^i = \begin{cases} \frac{\gamma}{n+\gamma} , & i = 0 \\ \frac{1}{2(n+\gamma)} , & i = 1 \dots 2n \end{cases} \quad (8)$$

- Calculate the mean and the covariance

$$\hat{X}_{k^-} = \sum_{i=0}^{2n} W^i \sigma_{f,k^-}^{i} \quad (9)$$

- Next, the observation covariance matrix

$$P_{zz,k} = \sum_{i=0}^{2n} W^i (\sigma_{h,k^-}^{i} - \hat{Y}_{k^-}) \times (\sigma_{h,k^-}^{i} - \hat{Y}_{k^-})^T \quad (10)$$

- On the other hand, the state/measurement cross covariance matrix

$$P_{xz,k} = \sum_{i=0}^{2n} W^i (\sigma_{f,k^-}^{i} - \hat{X}_{k^-}) \times (\sigma_{h,k^-}^{i} - \hat{Y}_{k^-})^T + R \quad (11)$$

- and then the Kalman gain is calculated by the equation:

$$K_k = P_{xz,k} P^{-1}{}_{zz,k} \quad (12)$$

- Finally, the updated states and covariance matrices are determined by:

$$X_{k^+} = \hat{X}_{k^-} + K_k(Y_k - C\hat{X}_{k^-})$$
$$P_{k^+} = P_{k^-} - [K_k P_{zz,k} K_k{}^T \quad (13)$$

3. Speed sensor fault-tolerant vector control

3.1 Speed sensor fault modelling

When the speed encoder is damaged, the measured signal can be modelled by a progressive bias on the real speed values due to the variations of the sensor internal parameters, its expression is as in Eq. (14) [20, 23]:

$$\omega_{rf} = \omega_r(1-\gamma) \quad (14)$$

Where ω_{rf} is the faulty measurement, ω_r is the real rotation speed and γ is the sensor gain.

For different values of γ, two kinds of faults can be distinguished:

Total sensor loss ($\gamma = [0, 1]$): This fault consists of cyclic interruptions of the sensor.

$$\omega_{rf} = \begin{cases} \omega_r & if \quad t < t_f \\ 0 & else \end{cases} \quad (15)$$

Where t_f represents the fault occurrence time.

Gain fault: This fault consists of a partial decrease in the actual rotation speed. Its expression is as follows:

$$\omega_{rf} = \begin{cases} \omega_r & if\ t < t_f \\ \left[1 - \frac{1}{\gamma}\left(1 - e^{-(t-t_f)}\right)\right]\omega_r, & else \end{cases} \quad (16)$$

3.2 Proposed speed fault detection and isolation strategy

The bloc diagram of the proposed fault-tolerant vector control structure is shown in the Fig. 1. It includes the IRFOC vector control strategy, the virtual observers (UKF or SMO given in the appendix), the physical speed encoder and the virtual fault-tolerant design.

The fault detection and isolation strategy of the speed sensor is based on the use of the non-linear state estimation observers (SMO or UKF). The detection algorithm consists of the following four steps (Fig. 1):

1. In the first step, the estimated and measured rotation speeds are compared to calculate the residuals (23):

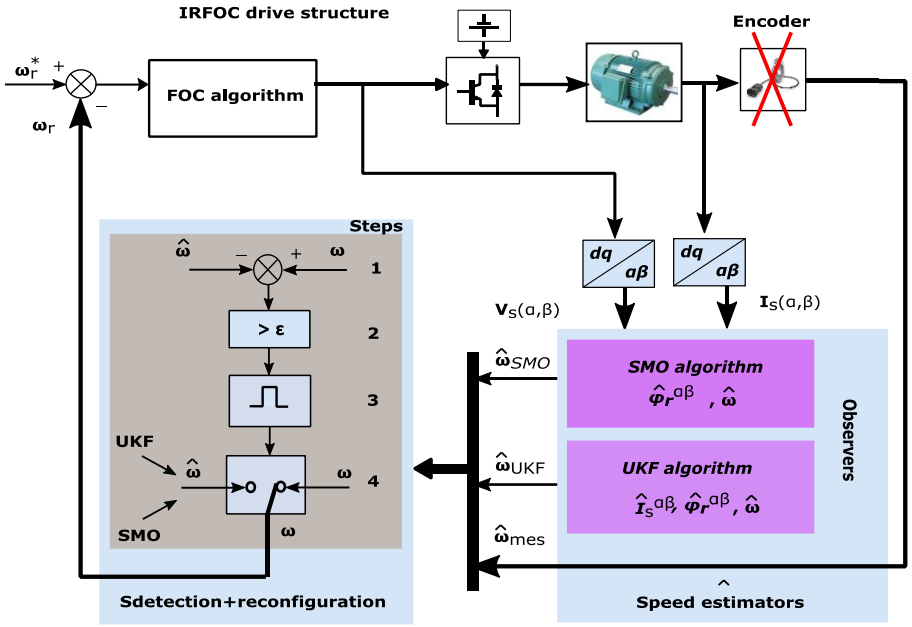

Figure. 1 Bloc diagram of the proposed FTC unit in the presence of broken speed sensor

$$\omega_{rf} = \begin{cases} \omega_r & if\ t < t_f \\ \left[1 - \frac{1}{\gamma}\left(1 - e^{-(t-t_f)}\right)\right]\omega_r & else \end{cases} \quad (17)$$

2. In the second step, the residuals are compared to the detection threshold. The threshold must be well chosen to maintain good performance and avoid false alarms. This is an important task that determines the minimum level of error that can be detected. They can be set experimentally on the basis of fault-free behaviour.

3. If the difference between these signals is greater than the threshold, a logic algorithm can detect speed sensor dysfunction.

$$F = \begin{cases} 1 & if \quad R_\omega - \varepsilon > 0 \\ 0 & else \quad R_\omega - \varepsilon \le 0 \end{cases} \quad (18)$$

4. The final step of the detector is to isolate the fault, if the fault is confirmed, by replacing the sensor with the speed estimator.

$$\omega_{rf} = \begin{cases} \omega_r & if \quad F = 0 \\ \hat{\omega}_r & else \quad F = 1 \end{cases} \quad (19)$$

4. Simulation and results

The implementation of the IRFOC vector control model has been performed in Matlab/Simulink (2013a) for a 1kW IM whose parameters are presented in the Table 1. The sampling time is chosen to be equal to $T_e = 10^{-5} sec$. To monitor the behavior of the system in case of speed sensor fault, the encoder will be subject to two types of faults: *Partial* and *total loss* of the speed sensor. To demonstrate the effectiveness of this solution over any given operating point, the simulation results were tested over a wide speed range (50→700→1475rpm).

Table 1. Parameters of the IM tested in the simulation

Parameter	Value
Voltage	400 V
Frequency	50 Hz
Stator winding resistance	6.8 Ω
Rotor winding resistance	5.43 Ω
Stator inductance	0.3978 H
Rotor inductance	0.3558 H
Mutual inductance	0.3558 H
Number of pole pairs	2
Total rotor inertia	0.02 kgm2
Fraction coefficient	0.0025 Nmsrad1

4.1 Impact of broken speed sensor

In order to illustrate the impact of the faulty speed sensor on the IRFOC IMD system, faults given by Eqs. (21) and (22) were applied for different operating points of the machine, in particular when the machine is working without load (Fig. 2 and 4) but also when the machine is loaded (Fig. 3 and 5). For each type of fault, a degraded behaviour is observed.

- Total sensor loss: This fault occurs at $t \in [6,27]s$ and was modelled by a periodic breaks/recovery (T=9s, α=60%) of the mechanical sensor signal. As soon as the fault is applied, the electromagnetic torque (in blue) reaches values greater than the maximum value that the machine

can tolerate (given in red) ($\approx C_{em}(F) > 4 * C_{em}(H)$) as shown in part (d) of Fig. 2 and 3. Moreover, as shown in part (c) of Fig. 2 and 3, the flux in the machine diverges and the speed of the machine is unknown (part (b) of Fig. 2 and 3). We no longer have any feedback on the speed, and it is no longer controlled. The system does not work correctly anymore and tends to diverge. Also, the estimated rotor speed quantities (by the UKF or the SMO) diverge due to the unobservability of the IM at zero speed (part (a) of Fig. 2 and 3).

On the other hand, when the sensor recovers its healthy state, the tracking of the reference speed trajectory shows large overshoots which is greater than two times the rated IM rotation speed leading to its destruction.

A shutdown is then imperative in order to preserve the IMD.

Gain fault: This fault occurs at $t \in [10,22]s$ and was modeled by a drop in sensor gain (-20%). When this fault appears, the speed feedback is erroneous (Fig. 4(a) and 5(a)) and then the rotation error is no longer negligible in both loaded (Fig. 5(b) and unloaded working conditions (Fig. 4(b)). The speed response estimation does not follow the reference speed and errors in the estimation are large (Fig. 4). The flux in the machine is no longer constant and does not reach the setpoint (Fig. 4(c) and 5(d)). The torque produced by the machine is varying correctly, but it shows non-negligibleripples which cause the vibration of the machine (Fig. 4(d) and 5(d)).

Uncertain and imprecise behavior of the system. Shutdown is desired.

4.2 Setting up the speed sensor fault-tolerant design

Two FTC versions are developed and compared. The first utilizes the UKF algorithm and the second is using the SMO algorithm. The detection threshold is set experimentally to $\varepsilon = 60$ rpm on the basis of a fault-free behavior to avoid false alarms. The effectiveness of the proposed FTC structures is tested in the presence of Gain fault and total sensor loss.

- Gain fault: A partial loss in the speed sensor signal (-20%) is applied at $t = 10s$. When the fault occurs, the measured rotor speed decreases (known as ω_f in part (a) of Fig. 8) and thus, the error between the measured and the estimated speed become higher than the threshold value ($R_{SMO} \& R_{UKF} \gg 60\,rpm$) as described in part (b) of Fig. 8. As a result, the detection flag F turns to 1 which indicates the occurrence of the fault (part (c)

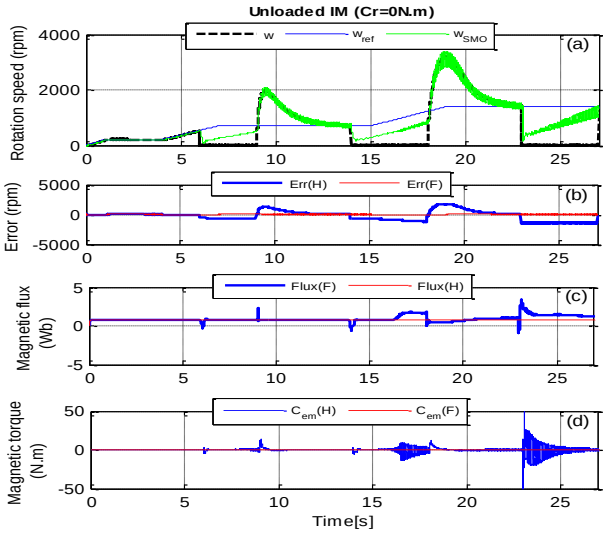

Figure. 2 Total loss of the speed sensor (duty cycle α=60%, period T=9s at t=6s) for no-loaded IM. Rotation speed (rpm) (a), rotation error (rpm) (b), Flux (Wb) (c) and the torque (N.m) (d). (F) and (H) are quantities in faulty and healthy operations, respectively

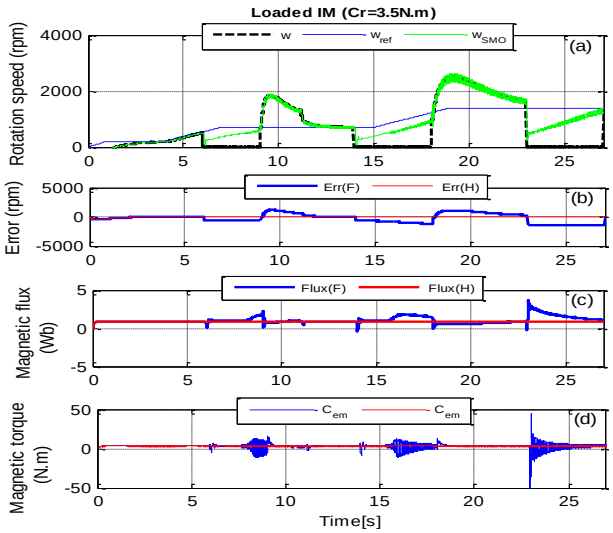

Figure. 3 Total loss of the speed sensor (duty cycle α=60%, period T=9s at t=6s) for loaded IM. Rotation speed (rpm) (a), rotation error (rpm) (b), Flux (Wb) (c) and the torque (N.m) (d)

of Fig. 8). Following this change, speed response feedback is quickly switched to the speed estimators presented by the UKF and SMO to maintain the stable behavior of the system. When the topology changes, an acceptable overshoot ($< 10\%$) appears on the IM states but the system maintain good performance in terms of stability and trajectory tracking. In the FTC design using the SMO algorithm, the reticence effect is visible at $t = 10s$ and for high-speed operation ($\omega_r \geq 1400$ rpm) as shown in the part (d) of Fig. 6. The part (a) of Fig. 7 demonstrates that the flux passing through the machine remains constant and equal to the set value.

The torque is quickly corrected and remains at 0 for unloaded condition (Fig. 7 part (b)).

- Total sensor loss: This fault occurs during $t \in [6, 27]s$. When the sensor signal information is lost, the flag goes to 1 and the reconfiguration action is activated. The speed feedback switches to analytical redundancy (UKF or SMO) to maintain operation. For this type of fault, the detection and isolation structure show good performance in terms of stability, overshoot rate, and trajectory tracking over the entire speed range (Fig. 8 and 9).

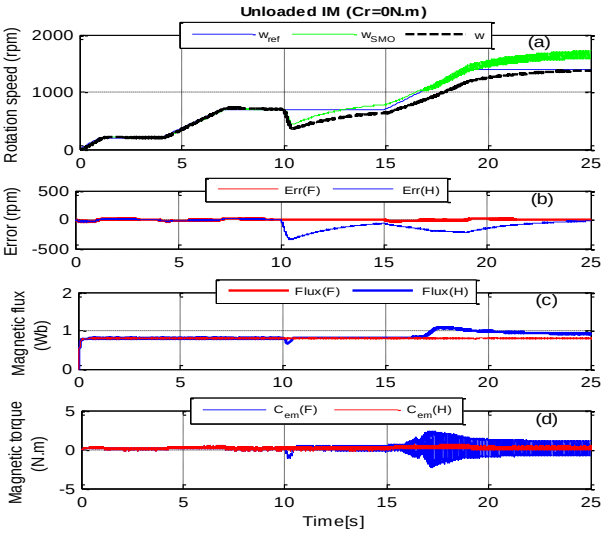

Figure. 4 Partial loss of the speed sensor (-20% gain at t=10s) for no-loaded IM. Rotation speed (rpm) (a), rotation error (rpm) (b), Flux (Wb) (c) and the torque (N.m) (d). (F) and (H) are quantities in faulty and healthy operations, respectively

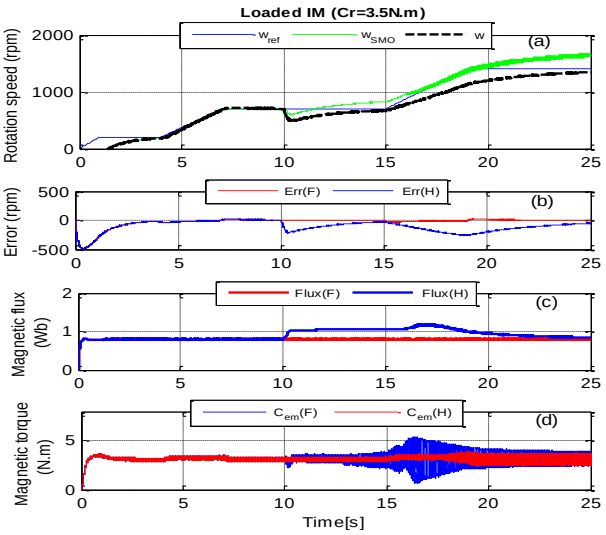

Figure. 5 Performance of the FTC strategy in case of a cyclic loss of the speed sensor (α=60%, T=9s at t=10s). Faulty rotation speed (a), Rotation error (b), detection flag (c), corrected rotor speed (d). (F) and (H) are quantities in faulty and healthy operations, respectively

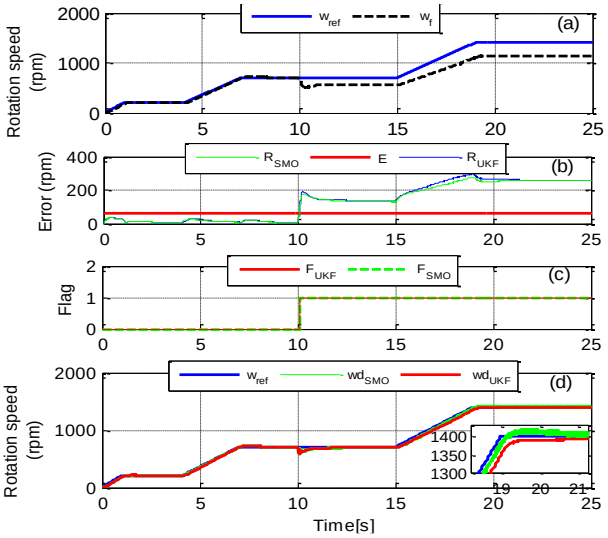

Figure. 6 Performance of the FTC unit in the case of gain fault (-20% at t=10s). Faulty rotation speed (a), Rotation error (b), detection flag (c), corrected rotor speed (d)

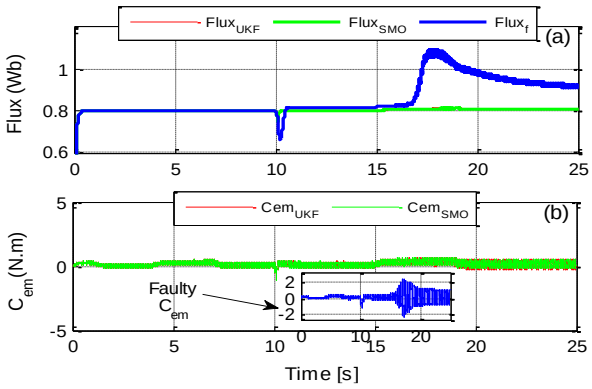

Figure. 7 Variations of magnetic quantities under gain fault. Flux (Wb) (a) and torque (N.m) (b)

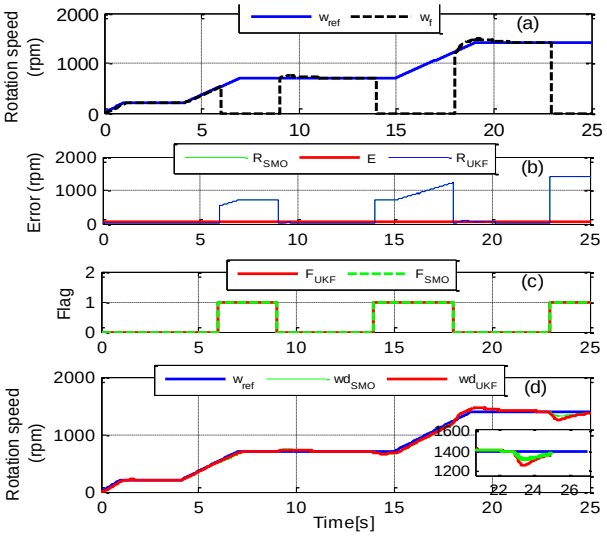

Figure. 8 Performance of the FTC unit in case of a cyclic loss of the speed sensor (α=60%, T=9s at t=10s). Faulty rotation speed (a), Rotation error (b), detection flag (c), corrected rotor speed (d)

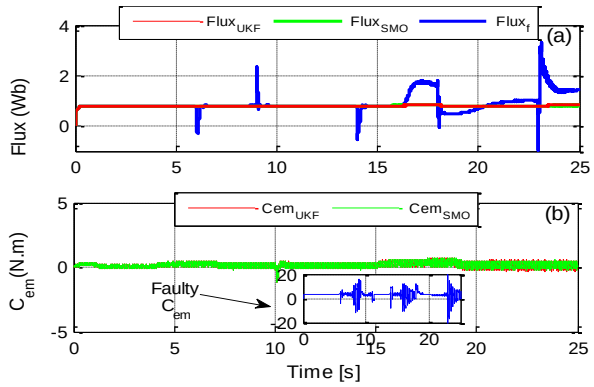

Figure. 9 Variations of magnetic quantities under cyclic total loss (α=60%, T=9s at t=10s) of the speed sensor. Flux (Wb) (a) and torque (N.m) (b)

5. Conclusion

In this paper, a novel virtual design for fault-tolerant vector control for IMD system with broken speed sensor has been proposed. This solution is based on the analytical redundancy algorithms (nonlinear UKF) to estimate, detect and compensate speed sensor faults in order to ensure the performance of the drive system. The validity of the proposed strategy was tested over the entire speed range, when the IM is loaded and loaded. The loss of the speed encoder is quickly detected and compensated. The proposed FTC design is simpler than the other diagnosis methods. Simulation results proved the superiority of the UKF over the SMO in terms of stability and speed trajectory tracking especially for high-speed range.

Conflicts of Interest

The authors declare no conflict of interest.

Author Contributions

Conceptualization, methodology, analysis, writing—original draft preparation, writing—review and editing has been done by 1st author. The visualization, supervision and project administration has been done by 2st author.

References

[1] Y. Liu, M. Stettenbenz, and A. Bazzi, "Smooth Fault-Tolerant Control of Induction Motor Drives with Sensor Failures", *IEEE Transactions on Power Electronics*, Vol. 34, No. 4, pp. 3544-3552, 2019.

[2] M. Manohar and S. Das, "Current Sensor Fault-Tolerant Control for Direct Torque Control of Induction Motor Drive Using Flux-Linkage Observer", *IEEE Transactions on Industrial Informatics*, Vol. 13, No. 6, pp. 2824-2833, 2017.

[3] M. Bouakoura, N. N. Said, and M. N. Said, "speed sensor faults diagnosis in an induction motor vector-controlled drive", *Acta Electrotechnica et Informatica*, Vol. 17, No. 1, pp. 49-57, 2017.

[4] A. Youssef, S. E. Khil, and I. S. Belkhodja, "State Observer-Based Sensor Fault Detection and Isolation, and Fault Tolerant Control of a Single-Phase PWM Rectifier for Electric Railway Traction", *IEEE Transactions on Power Electronics*, Vol. 28, No. 12, pp. 5842-5853, 2013.

[5] K. Klimkowski and M. Dybkowski, "A Fault Tolerant Control Structure for an Induction Motor Drive System", *Automatika*, Vol. 57, No. 3, pp. 638-647, 2016.

[6] C. Chakraborty and V. Verma, "Speed and Current Sensor Fault Detection and Isolation Technique for Induction Motor Drive Using Axes Transformation", *IEEE Transactions on Industrial Electronics*, Vol. 62, No. 3, pp. 1943-1954, 2015.

[7] Z. Gao, C. Cecati, and S. Ding, "A Survey of Fault Diagnosis and Fault-Tolerant Techniques—Part I: Fault Diagnosis with Model-Based and Signal-Based Approaches", *IEEE Transactions on Industrial Electronics*, Vol. 62, No. 6, pp. 3757-3767, 2015.

[8] K. Saad, K. Abdellah, H. Ahmed, and A. Iqbal, "Investigation on SVM-Backstepping sensorless control of five-phase open-end winding induction motor based on model reference adaptive system and parameter estimation", *Engineering Science and Technology, an International Journal*, Vol. 22, No. 4, pp. 1013-1026, 2019.

[9] M. Rayyam, M. Zazi, and Y. Barradi, "A new metaheuristic unscented Kalman filter for state vector estimation of the induction motor based on Ant Lion optimizer", *COMPEL - The International Journal for Computation and Mathematics in Electrical and Electronic Engineering*, Vol. 37, No. 3, pp. 1054-1068, 2018.

[10] M. Rayyam and M. Zazi, "A novel metaheuristic model-based approach for accurate online broken bar fault diagnosis in induction motor using unscented Kalman filter and ant lion optimizer", *Transactions of the Institute of Measurement and Control*, Vol. 42, No. 8, pp. 1537-1546, 2020.

[11] P. M. Frank, "Fault diagnosis in dynamic systems using analytical and knowledge-based

redundancy: A survey and some new results", *Automatica*, Vol. 26, No. 3, pp. 459-474, 1990.

[12] J. Su and W. Chen, "Model-Based Fault Diagnosis System Verification Using Reachability Analysis", *IEEE Transactions on Systems, Man, and Cybernetics: Systems*, Vol. 49, No. 4, pp. 742-751, 2019.

[13] A. Teja, V. Verma, and C. Chakraborty, "A New Formulation of Reactive-Power-Based Model Reference Adaptive System for Sensorless Induction Motor Drive", *IEEE Transactions on Industrial Electronics*, Vol. 62, No. 11, pp. 6797-6808, 2015.

[14] V. Vasic, S. Vukosavic, and E. Levi, "A stator resistance estimation scheme for speed sensorless rotor flux-oriented induction motor drives", *IEEE Transactions on Energy Conversion*, Vol. 18, No. 4, pp. 476-483, 2003.

[15] Z. Yan, C. Jin, and V. Utkin, "Sensorless sliding-mode control of induction motors", *IEEE Transactions on Industrial Electronics*, Vol. 47, No. 6, pp. 1286-1297, 2000.

[16] A. Amin and K. Hasan, "A review of Fault Tolerant Control Systems: Advancements and applications", *Measurement*, Vol. 143, pp. 58-68, 2019.

[17] A. Raisemche, M. Boukhnifer, C. Larouci, and D. Diallo, "Two Active Fault-Tolerant Control Schemes of Induction-Motor Drive in EV or HEV", *IEEE Transactions on Vehicular Technology*, Vol. 63, No. 1, pp. 19-29, 2014.

[18] Y. Azzoug, A. Menacer, R. Pusca, R. Romary, T. Ameid, and A. Ammar, "Fault Tolerant Control for Speed Sensor Failure in Induction Motor Drive based on Direct Torque Control and Adaptive Stator Flux Observer", In: *Proc. of International Conference on Applied and Theoretical Electricity*, pp. 1-6, 2018.

[19] A. Raisemche, M. Boukhnifer, and D. Diallo, "New fault-tolerant control architectures based on voting algorithms for electric vehicle induction motor drive", *Transactions of the Institute of Measurement and Control*, Vol. 38, No. 9, pp. 1120-1135, 2015.

[20] M. Adamczyk and T. O. Kowalska, "Virtual Current Sensor in the Fault-Tolerant Field-Oriented Control Structure of an Induction Motor Drive", *Sensors*, Vol. 19, No. 22, 2019.

[21] A. Derdiyok, M. Guven, H. Rehman, N. Inanc, and L. Xu, "Design and implementation of a new sliding-mode observer for speed-sensorless control of induction machine", *IEEE Transactions on Industrial Electronics*, Vol. 49, No. 5, pp. 1177-1182, 2002.

[22] S. Jafarzadeh, C. Lascu, and M. S. Fadali, "State Estimation of Induction Motor Drives Using the Unscented Kalman Filter", *IEEE Transactions on Industrial Electronics*, Vol. 59, No. 11, pp. 4207-4216, 2013.

[23] D. C. Delgado, D. E. Trejo, and E. Palacios, "Fault-tolerant control in variable speed drives: a survey", *IET Electric Power Applications*, Vol. 2, No. 2, pp. 121-134, 2008.